Received 8 December 2022; revised 11 January 2023; accepted 12 January 2023. Date of publication 17 January 2023; date of current version 1 February 2023.
Digital Object Identifier 10.1109/OJAP.2023.3237728

Wideband 3-D Printed All-Metal Reflectarray With Notches for Low-Cost Millimeter-Wave Applications

XIAOWEI CAO [1] (Graduate Student Member, IEEE), CHANGJIANG DENG [1,2] (Senior Member, IEEE), YINAN HAO [1], AND YOUJIA YIN [1]

[1] Beijing Key Laboratory of Millimeter Wave and Terahertz Technology, School of Integrated Circuits and Electronics, Beijing Institute of Technology, Beijing 100081, China

[2] Tangshan Research Institute, Beijing Institute of Technology, Tangshan 063099, China

CORRESPONDING AUTHOR: C. DENG (e-mail: dengcj11@bit.edu.cn)

This work was supported by the National Natural Science Foundation of China under Contract 62071037.

ABSTRACT In this paper, a 3-D printed all-metal reflectarray is presented for millimeter-wave applications. The array has sub-wavelength element spacing, so that the elements are non-resonant. A two-stage notch is etched at the top of the element, which provides multiple degrees of freedom for phase tuning. The phase variation range is more than 360° by changing the height and width of the first stage of the notch. Thanks to the non-resonant property and the two-stage notching, stable phase shift can be maintained in wide frequency range. A reflectarray with 20×20 elements is fabricated by using 3-D printing technique, which has the merits of flexible construction, light weight and low cost. The simulated and measured results on radiation patterns and realized gain are highly consistent. The measured 1-dB gain bandwidth achieves 17.6%, ranging from 31 GHz to 37 GHz. In the whole 1-dB gain bandwidth, the measured aperture efficiency is higher than 47.7%, with a peak efficiency of 53.6% at 31 GHz. The proposed reflectarray has no substrate loss and can provide high aperture efficiency in wide bandwidth.

INDEX TERMS Metal reflectarray, wideband, high aperture efficiency, 3-D printing.

I. INTRODUCTION

NOWADAYS, there is a widespread and increasing interest in metaverse, which uses virtual world and virtual objects for entertainment, education, training, and research applications. To support high wireless transmission rate in metaverse, wide bandwidth is needed [1], [2]. Millimeter wave (mm-wave) band is promising for metaverse applications due to its wide bandwidth and small size of devices.

High gain antennas are needed to overcome the drawback of large path loss in mm-wave band [3]. Phased arrays [4], [5], parabolic reflectors [6], [7], and reflectarrays [8], [9] are the typical antenna structures to generate high gain beam. Among them, reflectarray is attractive because it combines the merits of phased arrays and reflectors, which has flexible element configuration and spatial feed simultaneously. Therefore, reflectarrays have low cost, low profile and high efficiency [10]. The elements of the reflectarrays have various types, such as microstrip patch, dipole, slot, dielectric resonant antenna, waveguide. The fabrication of the reflectarray is also flexible, including printed circuit board (PCB) etching, 3-D dielectric or metal printing, and low temperature co-fired ceramic (LTCC) and MEMS micromachining techniques [11], [12], [13], [14], [15].

Microstrip reflectarrays using PCB technique are popular owing to planar structure and ease of fabrication. Various designs have been proposed [16], [17], [18]. However, microstrip reflectarrays have both dielectric loss and conductor loss. The radiation efficiency will decrease when the frequency increases to mm-wave and Terahertz bands [19]. All-dielectric reflectarrays [20], [21], [22] and all-metal reflectarrays [23], [24], [25] are then designed to reduce loss. Metal reflectarray is preferred in applications that have harsh environment due to its mechanical robustness. For example, a metal-only reflectarray is presented in [24]. The 1-dB gain bandwidth is 8.3%. These metal-only designs are similar to microstrip reflectarrays except that the dielectric layer is replaced by air layer.

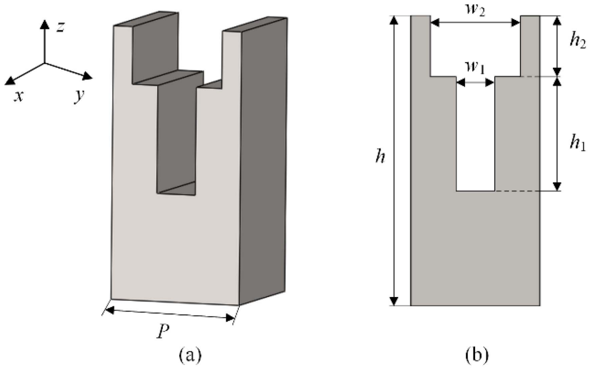

FIGURE 1. Configuration of the proposed element. (a) 3-D view. (b) Side view.

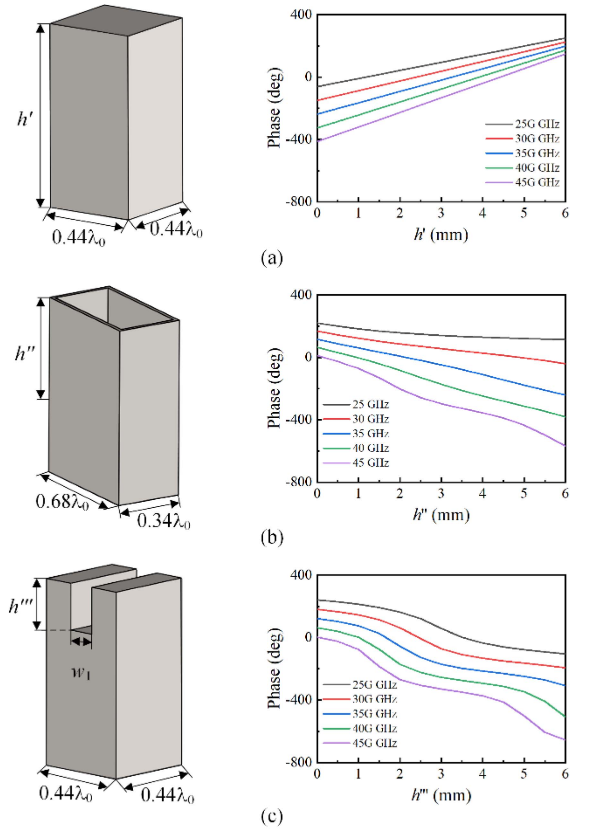

FIGURE 2. Three kinds of all-metal elements and simulated reflection phase. (a) Metal block with different heights. (b) Waveguide with different depth. (c) Notched element with different depth.

In mm-wave band, it is possible to utilize the 3-D structure, not only the 2-D structure, to develop reflectarray that has high performance. As the wavelength becomes small, the drawback of bulky volume and heavy weight can be ignored. Lots of all- metal reflectarrays have been presented [26], [27], [28], [29], [30], [31], [32], [33], [34]. Waveguide element is one of the most popular 3-D structures [26], [27], [28]. For instance, the first waveguide reflectarray design proposed in 1963 [26]. The reflected phase is shifted by changing the suffers from narrow bandwidth, since the phase shift is highly related to frequency. To increase the bandwidth, non-resonant 3-D structures are proposed, such as metal blocks [26], [27], [28] and grooves [32], [33], [34]. For example, a metal-only reflectarray using metal block is proposed in [29]. The 1-dB gain bandwidth achieves 13.4%.

Recently, 3-D metal printing technique has been introduced in mm-wave antenna designs, which has the merits of low cost and flexible construction ability [35]. In 2016, an all-metal waveguide reflectarray is presented [36]. The metallization of the element is achieved via electroplating. In 2020, a high-gain filtering reflectarray is designed using 3-D printing technique [37]. The aperture efficiency is 40.5%. In [38], a 3-D printed Phoenix cell with wide bandwidth is designed at 20 GHz. The cell consists of a metal block and two concentric waveguides, which leads to very thin walls. It is difficult to scale down the structure to higher frequency regime.

In this paper, a high gain high efficiency metal reflectarray is presented using 3-D metal printing technique. A two-stage notch is etched in each element. The phase shift range is larger than 360° by changing the depth of the notch. Stable phase response is maintained in wide frequency range. The novelty is summarized as follows. Firstly, the element is non-resonant, which is less sensitive to frequency variation than waveguide. Secondly, the period is sub-wavelength, which has small phase quantization error. Thirdly, the two-stage notch provides multiple freedom to enhance the bandwidth. Finally, the reflectarray is all metal, and is made by 3-D printing, which has low fabrication cost and flexible construction ability.

II. UNITS

Fig. 1 shows the geometry of the proposed all-metal element. The size of the element is 4×4 mm^2, corresponding to $0.44 \times 0.44\ \lambda_0^2$ at 33 GHz. A two-stage notch is etched along *x*-axis. The depth and width of the notch are optimized to obtain stable phase response in wide frequency band. The element is single linear polarized, whose polarization is along y-axis.

In order to depict the advantage of the proposed element in phase shift, three types of elements are compared, including metal block, waveguide, and the one-stage notched element. As shown in Fig. 2, the metal block and the notched element have the same size, while the waveguide has the size of $0.68 \times 0.34\ \lambda_0^2$. It implies that the waveguide is resonant and operates at TE_{10} mode, while the metal block and the notched element are non-resonant. The height of the metal block, the depth of the waveguide and the depth of the notched element are used to change the value of the reflection phase, respectively.

The reflection phases of the three elements are shown at the right part of Fig. 2. All the elements have the same tuning distance of depth or height for fair comparison. As the notched depth or height sweeps from 0 mm to 6 mm, the phase variation of waveguide or block element is small at 25 GHz, but large at 40 GHz. The phase response curves are not parallel under different frequencies. It means that the

TABLE 1. Phase variation range at different frequencies.

Unit type	25GHz	30GHz	35GHz	40GHz
Block	259°	312°	364°	415°
Waveguide	99°	172°	294°	377°
Notched	**318°**	**345°**	**370°**	**408°**

TABLE 2. Detailed dimensions of the four states (unit: mm).

	One-stage notch (H_2= 0, W_2= 0)		Two-stage notch (h_2= 1.6, w_2= 2.8)	
	h_1	w_1	h_1	w_1
State 1	1.8	1.8	1.2	1.1
State 2	2.8	2.7	1.8	2
State 3	3.5	1.8	2.9	2.1
State 4	5.7	1.6	4	1.2

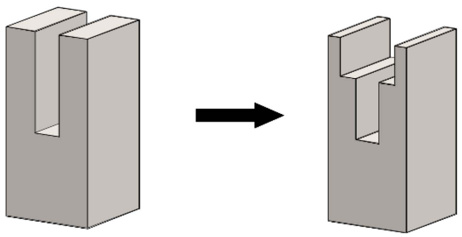

FIGURE 3. Evolution from one-stage notch to two-stage notch.

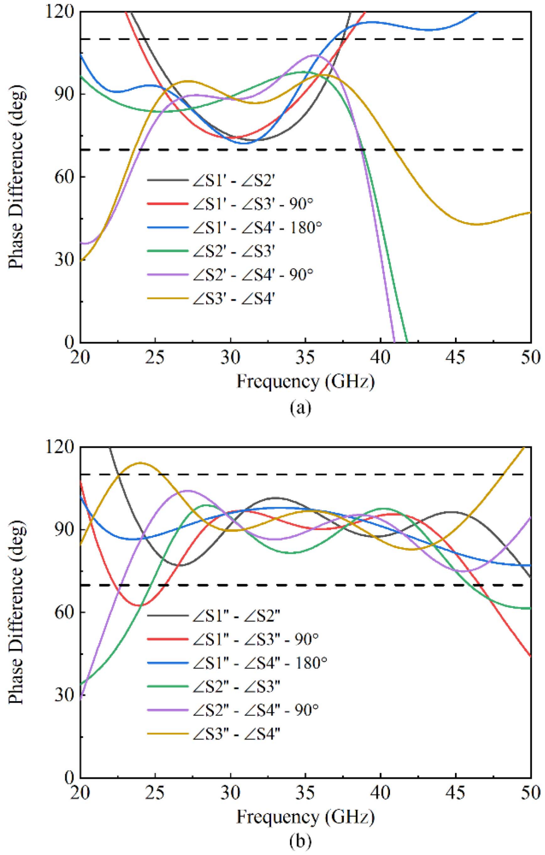

FIGURE 4. Simulated reflection phase difference of the two elements with 2-bit resolution. (a) One-stage notch. (b) Two-stage notch.

phase of the two types is sensitive to frequency variation, thus the available bandwidth is narrow. On the contrary, in the proposed element, the phase curves are nearly parallel, as the frequency changes. To quantitively evaluate the phase performance of the three types, the data extracted from Fig. 2 is listed in the Table 1. The phase shift range of the notched element keeps around 360° in the whole frequency band (25-45 GHz). The properties of sub-wavelength element spacing and two-stage notching lead to a wide band element for reflectarray design.

Based on the one-stage notch, two-stage notch is analyzed to further increase the stability of phase shift in wide frequency band. As shown in Fig. 3, the two notches have the same depth, but the two-stage notch has more parameters to tune the phase response, indicating the potential of wide bandwidth.

The two-stage notch has four parameters (h_1, h_2, w_1, w_2) that can be changed. It increases the flexibility of phase tuning, but the optimization process becomes complex. In order to reduce the complexity, the continuous phase shift is dispersed into several discrete states. According to the analysis in [39], the quantization loss caused by 1-bit, 2-bit, and 3-bit discretization is about 3 dB, 0.6 dB, and 0.2 dB, respectively. Take the design complexity, the quantization loss, and the fabrication accuracy into account, 2-bit resolution is adopted to verify the design. Table 2 lists the optimized values of the four states, which correspond to 0°, 90°, 180°, and 270° phase shift. Only two parameters (h_1, w_1) are changed to simplify the design.

The performances of the one-stage and two-stage notches are compared with 2-bit resolution. Fig. 4 shows the reflection phase difference between any two states. Ideal 90° or 180° is subtracted in some curves. For the one-stage notch, the phase difference maintains 90±20° in the 24-36 GHz band. For the two-stage notch, the phase difference is within 90±20° in 26-47 GHz band. The relative bandwidth of the two-stage notched element is greatly improved.

Parametric analysis is carried out to analyze the influence of the notch on reflection phase. As shown in Fig. 5, the depth of the notch can change the variation range of the reflection phase curve, especially h_1. On the other hand, the width of the notch can change the linearity of the reflection phase curve. To be specific, w_1 and w_2 changes the slope of the curve at 33 GHz and 39 GHz, respectively. Therefore, parametric studies reveal that the two-stage notch can effectively tune the phase of the reflection coefficient.

The reflection magnitude of the element in different states is shown in Fig. 6. The reflection magnitude is close to 0 dB in all the states, which means that almost full reflection is achieved. The reason of high efficiency is that the model is made of metal and no dielectric loss exists.

The mechanism of achieving wideband is analyzed. Fig. 7 illustrates the operating principle from the perspective of

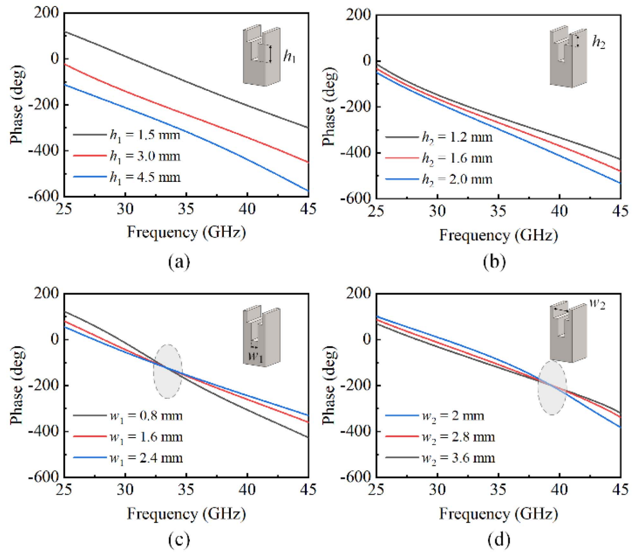

FIGURE 5. Influence of the notch on the reflection phase by changing (a) h_1, (b) h_2, (c) w_1, (d) w_2.

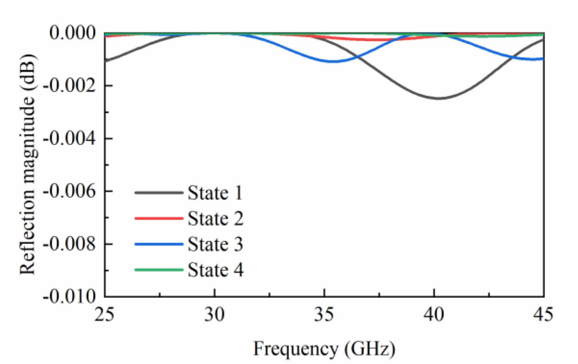

FIGURE 6. Reflection magnitude of the proposed element in different states.

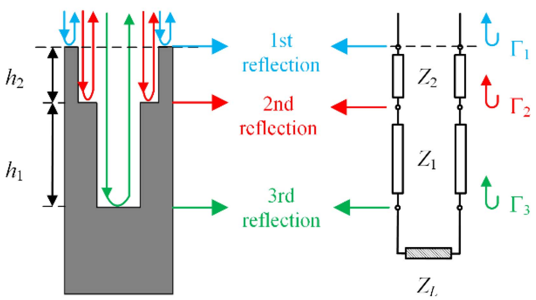

FIGURE 7. Conceptual explanation of the multi-reflection element.

multiple reflections [40]. The two-stage notch introduces three reflections at different depths. According to transmission line theory, the input impedance of a transmission line is

$$Z_{\text{in}} = Z_0 \times \frac{[Z_L + jZ_0 \tan(\beta h)]}{[Z_0 + jZ_L \tan(\beta h)]} \tag{1}$$

where Z_L is the impedance of the terminal load, Z_0 and h are the characteristic impedance and length of the transmission line, respectively. Z_L equals to zero, when the load is short-circuited. Then, the equation is simplified

$$Z_{\text{in}} = jZ_0 \tan(\beta h) \tag{2}$$

The reflection coefficient at the input port is

$$\Gamma = \frac{Z_{\text{in}} - Z_0}{Z_{\text{in}} + Z_0} = \frac{jZ_0 \tan(\beta h) - Z_0}{jZ_0 \tan(\beta h) + Z_0} = -e^{-2j\beta h} \tag{3}$$

From this equation, it is known that the reflection phase is determined by the notched depth. In the proposed element, the model can be viewed as a transmission line with three-stage reflections. So the total reflection coefficient (Γ_Σ) is written as

$$\Gamma_\sum = \Gamma_1 + \Gamma_2 e^{-2j\beta_2 h_2} + \Gamma_3 e^{-2j\beta_2 h_2} e^{-2j\beta_1 h_1} \tag{4}$$

where Γ_1, Γ_2, Γ_3 is the reflection amplitude at each stage, which is controlled by the notched width.

The element works as a multi-stage impedance transformer. It should have wider bandwidth than the one-stage transformer, because the proposed model has more degrees of freedom for optimization, which has already been indicated in Fig. 4. This is another reason of wideband performance, apart from the sub-wavelength element spacing.

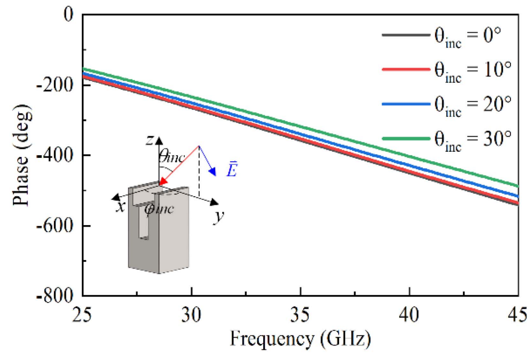

FIGURE 8. Reflection phase under different incident angles.

The effect of oblique incidence on phase shift is depicted in Fig. 8. Stable phase response is observed in the frequency band, when the incident angle sweeps from 0° to 30°. As the incident angle of the reflectarray is designed to be within 30°, the phase is little changed under different incident angles.

III. EXPERIMENTAL RESULTS

A reflectarray with 20×20 elements is designed based on the notched element. Standard horn antenna operating at 26.5-40 GHz band is adopted as the feeder, which has the gain of 21.4 dBi at 33 GHz. The feeder is 25° offset from the z-axis. The ratio of the focal distance to the diameter of the array (F/D) is 2.6, considering the trade-off between illumination efficiency and spillover efficiency.

According to the theory of reflectarray design, the phase of the mn-th element can be calculated as

$$\phi_{com,mn} = k_0 \times d_{mn} + \varphi_{req,mn} + \Delta\varphi \tag{5}$$

where k_0 is the wavenumber in free space, d_{mn} is the distance between the phase center of the feed and the mn-th element,

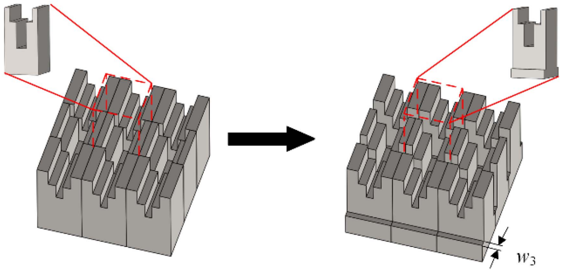

FIGURE 9. Evolution of the array elements.

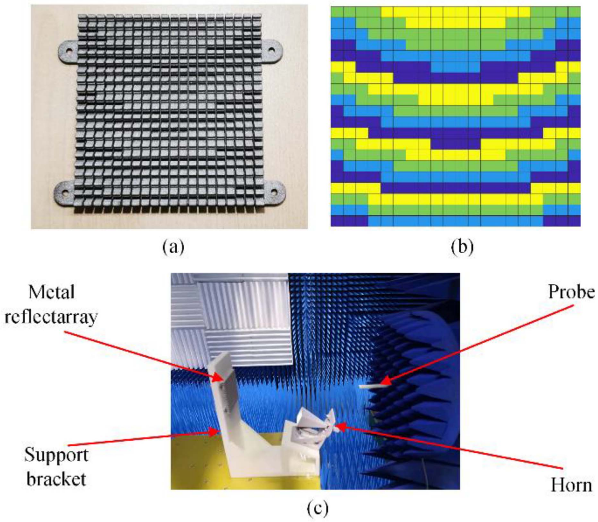

FIGURE 10. Prototype of the reflectarray. (a) Photograph. (b) Phase distribution. (c) Measurement setup.

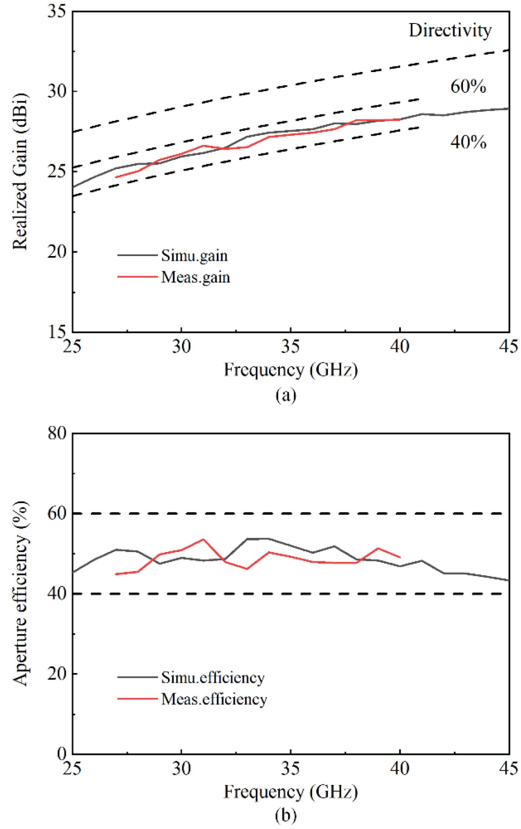

FIGURE 11. Simulated and measured gains and aperture efficiencies of the proposed reflectarray.

$\varphi_{req,mn}$ is the required phase when the main beam points to the angle of (φ_r, θ_r). $\Delta\varphi$ is a phase constant that provides an additional degree to optimize the phase distribution of the array, and increases the aperture efficiency.

In the simulation of unit cell, periodic boundary is used, which means that the notched depths of adjacent elements are the same. However, in reflectarray design, the notched depths of adjacent elements are different, since the phase distribution is not uniform. Therefore, one may think that the unit model is not accurate, and some elements are similar to waveguides when the notches are blocked by adjacent elements. In order to eliminate these concerns, the unit model is slightly modified. As shown in Fig. 9, narrow grooves with 0.5mm width (w_3) are periodically etched between adjacent elements along the x-direction to isolate the elements, so that all the notches will not be blocked by the neighbor ones. By comparing the results of the two models, it is found that both models have similar reflection behaviors. Therefore, the operating mechanism of the proposed element is different from that of waveguide, and the unit model can be used to analyze the performances of the reflectarray.

The prototype of the proposed reflectarray is fabricated by using low-cost 3-D metal printing technique. Fig. 10 shows the photograph and phase distribution of the reflectarray. 3-D metal printing facility developed by ZRapid Tech Company is employed for the array's fabrication. The axis resolution of the printer is 0.2 mm. The thickness of the layer can be reduced to 0.05 mm by decreasing the printing speed. Aluminum alloy AlSi10Mg powder is chosen as the printing material, due to the small grain size of the spherical metal powder. The diameter of the metal powder is between 15~53 μm. The cost of the fabrication is less than 100 US dollar. The aperture size of the reflectarray is 80×80 mm^2 (8.8×8.8 λ_0^2, λ_0 is the wavelength at 33 GHz in free space). A 2.5-mm-thick metal base is used to enhance the mechanical strength. This modification has little effect on the performance.

The radiation patterns of the reflectarray are measured in a near-field chamber. Fig. 11 shows the simulated and measured gain and aperture efficiency of the reflectarray. The measured frequency is from 27 GHz to 40 GHz, due to the limitation of the chamber. Good agreement is observed between the simulated and measured data. The measured gain is around 25 dBi. The 1-dB gain bandwidth is about 17.6%, ranging from 31 GHz to 37 GHz. It is observed that both the directivity and the gain increase as the frequency increases. A more accurate evaluation for wideband high gain antenna is using the aperture efficiency, which is calculated as

$$\eta = \frac{\lambda^2 G}{(4\pi \times A_p)} \tag{6}$$

where G is the peak gain, and A_p is the physical aperture area of the reflectarray.

TABLE 3. Comparisons of the proposed design with referenced all-metal reflectarrays.

Ref.	Element	1-dB gain BW (%)	Fabrication	Gain (dBi)	AE (%)	SLL (dB)	X- pol. (dB)	Aperture size (λ_0^2)	F/D	Polarization
[23]	Slot	6.8	Machining	31.4	35.0	-24	NG	$10^2\times\pi$	0.94	Dual CP
[24]	Slot	8.3	Machining	32.5	39.0	-22	-20	$10.75^2\times\pi$	0.81	Dual LP
[25]	Slot	12.8	Machining	33.9	53.8	-21	-35.3	$10.75^2\times\pi$	0.77	Single LP
[29]	Block	13.4*	Machining	28.0	50.1	-20	NG	10×10	0.75	Dual LP
[31]	Block	10.6	Machining	37.2	44.8	-14	NG	$15.65^2\times\pi$	0.6	Dual LP
[32]	Groove	7.3*	Machining	34.2	40.4	-11	NG	22×22	0.6	Single LP
[40]	Notch	6.4*	Machining	18.9	16.7	-10	-20	6.1×6.1	0.57	Single LP
[37]	Waveguide	12.5*	3-D printing	27.9	40.5	-17	-26.4	11×11	0.5	Single LP
Props.	**Notch**	**17.6**	**3-D printing**	**26.5**	**53.6**	**-15**	**-22**	**8.8×8.8**	**2.6**	**Single LP**

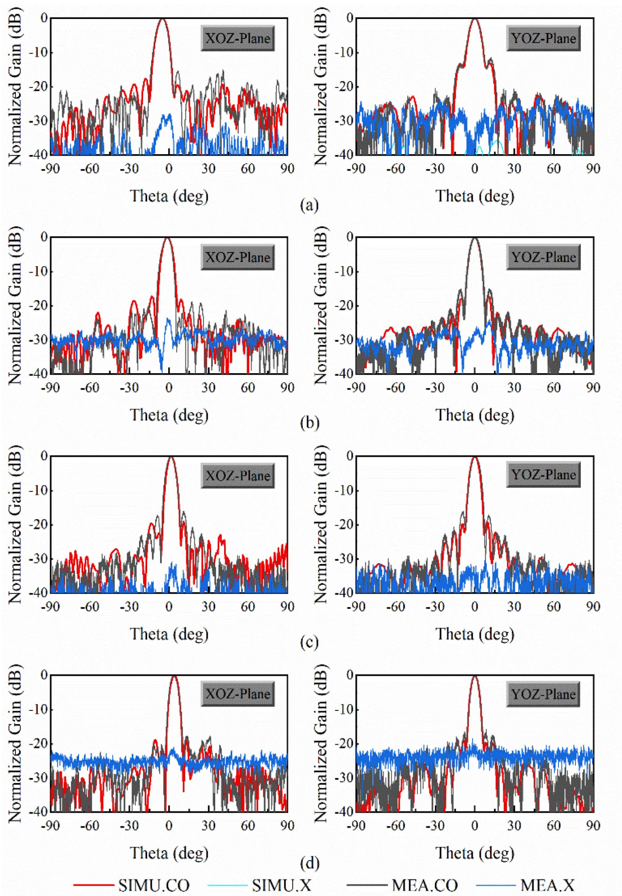

FIGURE 12. Simulated and measured normalized radiation patterns. (a) 27GHz. (b) 31GHz. (c) 35GHz. (d) 39GHz.

Based on this equation, the simulated and measured aperture efficiencies are calculated. As shown in Fig. 11(b), the measured peak aperture efficiency achieves 53.6% at 31 GHz. The aperture efficiency is higher than 47.7% in the whole 1-dB gain bandwidth. The discrepancy between the simulated and measured data is mainly caused by fabrication and measurement errors.

Fig. 12 shows the normalized radiation patterns in the *xoz* and *yoz* planes at four representative frequency points. It is shown that the simulated and measured radiation patterns agree well. Pencil beam is observed at all the four points. The measured side lobe level (SLL) is below –15 dB at all the frequency points. Slight beam squint is observed when the frequency changes, which can be reduced by optimizing the location of the feeder or using two feeders [41], [42].

Table 3 compares the performances of the proposed antenna with other all-metal reflectarray antennas. Compared with the referenced designs, the proposed reflectarray has wider 1-dB gain bandwidth and higher aperture efficiency. In addition, the fabrication of the proposed prototype is based on 3-D printing technique, thus the cost is low.

IV. CONCLUSION

In this paper, a wideband 3-D printed metal reflectarray is investigated for mm-wave applications. By etching two-stage notch in each element, stable reflection phase shift is achieved in wide frequency range. The widths and depths of the notch provide multiple degrees of freedom to optimize the bandwidth. The all-metal reflectarray is fabricated by using 3-D metal printing. The measured 1-dB gain bandwidth covers 31-37 GHz band, and the aperture efficiency is higher than 47.7% in the entire gain bandwidth. The proposed reflectarray has the merits of low cost, wide bandwidth, and high aperture efficiency, which is promising for metaverse applications.

REFERENCES

[1] L. Chang et al., "6G-enabled edge AI for metaverse: Challenges, methods, and future research directions," *J. Commun. Inf. Netw.*, vol. 7, no. 2, pp. 107–121, Jun. 2022.

[2] A. M. Al-Ghaili et al., "A review of metaverse's definitions, architecture, applications, challenges, issues, solutions, and future trends," *IEEE Access*, vol. 10, pp. 125835–125866, 2022.

[3] Y. You, Y. Lu, Q. You, Y. Wang, J. Huang, and M. J. Lancaster, "Millimeter-wave high-gain frequency-scanned antenna based on waveguide continuous transverse stubs," *IEEE Trans. Antennas Propag.*, vol. 66, no. 11, pp. 6370–6375, Nov. 2018.

[4] W. Sun, Y. Li, L. Chang, H. Li, X. Qin, and H. Wang, " Dual-band dual-polarized microstrip antenna array using double-layer gridded patches for 5G millimeter-wave applications," *IEEE Trans. Antennas Propag.*, vol. 69, no. 10, pp. 6489–6499, Oct. 2021.

[5] H. Li, Y. Li, L. Chang, W. Sun, X. Qin, and H. Wang, "A wideband dual-polarized endfire antenna array with overlapped apertures and small clearance for 5G millimeter-wave applications," *IEEE Trans. Antennas Propag.*, vol. 69, no. 2, pp. 815–824, Feb. 2021.

[6] Z.-Y. Zhang, Y. Zhao, N.-W. Liu, L.-Y. Ji, S. Zuo, and G. Fu, "Design of a dual-beam dual-polarized offset parabolic reflector antenna," *IEEE Trans. Antennas Propag.*, vol. 67, no. 2, pp. 712–718, Feb. 2019.

[7] G. Mishra, S. K. Sharma, and J.-C.-S. Chieh, "A circular polarized feed horn with inbuilt polarizer for offset reflector antenna for W-band CubeSat applications," *IEEE Trans. Antennas Propag.*, vol. 67, no. 3, pp. 1904–1909, Mar. 2019.

[8] Z. Cao, Y. Li, Z. Zhang, and M. F. Iskander, "Single motor-controlled mechanically reconfigurable reflectarray," *IEEE Trans. Antennas Propag.*, vol. 71, no. 1, pp. 190–199, Jan. 2023, doi: 10.1109/TAP.2022.3221036.

[9] W. Zhang, Y. Li, and Z. Zhang, "A reconfigurable reflectarray antenna with an 8 μm-thick layer of liquid crystal," *IEEE Trans. Antennas Propag.*, vol. 70, no. 4, pp. 2770–2778, Apr. 2022.

[10] Y. Li, Z. N. Chen, X. Qing, Z. Zhang, J. Xu, and Z. Feng, "Axial ratio bandwidth enhancement of 60-GHz substrate integrated waveguide-fed circularly polarized LTCC antenna array," *IEEE Trans. Antennas Propag.*, vol. 60, no. 10, pp. 4619–4626, Oct. 2012.

[11] L. Dai et al., "Reconfigurable intelligent surface-based wireless communications: Antenna design, prototyping, and experimental results," *IEEE Access*, vol. 8, pp. 45913–45923, 2020.

[12] L. Chang, Y. Li, Z. Zhang, X. Li, S. Wang, and Z. Feng, "Low-sidelobe air-filled slot array fabricated using silicon micromachining technology for millimeter-wave application," *IEEE Trans. Antennas Propag.*, vol. 65, no. 8, pp. 4067–4074, Aug. 2017.

[13] L. Chang, Y. Li, Z. Zhang, S. Wang, and Z. Feng, "Planar air-filled terahertz antenna array based on channelized coplanar waveguide using hierarchical silicon bulk micromachining," *IEEE Trans. Antennas Propag.*, vol. 66, no. 10, pp. 5318–5325, Oct. 2018.

[14] L. Chang, Z. Zhang, Y. Li, S. Wang, and Z. Feng, "Air-filled long slot leaky-wave antenna based on folded half-mode waveguide using silicon bulk micromachining technology for millimeter-wave band," *IEEE Trans. Antennas Propag.*, vol. 65, no. 7, pp. 3409–3418, Jul. 2017.

[15] P. Liu, Y. Li, Z. Zhang, S. Wang, and Z. Feng, "A fixed-beam leaky-wave cavity-backed slot antenna manufactured by bulk silicon MEMS technology," *IEEE Trans. Antennas Propag.*, vol. 65, no. 9, pp. 4399–4405, Sep. 2017.

[16] X. Pan, F. Yang, S. Xu, and M. Li, "A 10 240-element reconfigurable reflectarray with fast steerable monopulse patterns," *IEEE Trans. Antennas Propag.*, vol. 69, no. 1, pp. 173–181, Jan. 2021.

[17] F. Wu, R. Lu, J. X. Wang, Z. H. Jiang, W. Hong, and W.-M. Luk, "A circularly polarized 1 bit electronically reconfigurable reflectarray based on electromagnetic element rotation," *IEEE Trans. Antennas Propag.*, vol. 69, no. 9, pp. 5585–5595, Sep. 2021.

[18] J. Han, L. Li, G. Liu, Z. Wu, and Y. Shi, "A wideband 1 bit 12 × 12 reconfigurable beam-scanning reflectarray: Design, fabrication, and measurement," *IEEE Antennas Wireless Propag. Lett.*, vol. 18, no. 6, pp. 1268–1272, Jun. 2019.

[19] E.-C. Choi and S. Nam, "High-efficiency dielectric reflectarray antennas with ultra-wideband characteristics," *IEEE Access*, vol. 9, pp. 152075–152081, 2021.

[20] B. Li, C. Y. Mei, Y. Zhou, and X. Lv, "A 3-D-printed wideband circularly polarized dielectric reflectarray of cross-shaped element," *IEEE Antennas Wireless Propag. Lett.*, vol. 19, no. 10, pp. 1734–1738, Oct. 2020.

[21] Y. X. Sun, D. Wu, and J. Ren, "Millimeter-wave dual-polarized dielectric resonator reflectarray fabricated by 3D printing with high relative permittivity material," *IEEE Access*, vol. 9, pp. 103795–103803, 2021.

[22] Q. Cheng et al., "Dual circularly polarized 3-D printed broadband dielectric reflectarray with a linearly polarized feed," *IEEE Trans. Antennas Propag.*, vol. 70, no. 7, pp. 5393–5403, Jul. 2022.

[23] K. Q. Henderson and N. Ghalichechian, "Circular-polarized metal-only reflectarray with multi-slot elements," *IEEE Trans. Antennas Propag.*, vol. 68, no. 9, pp. 6695–6703, Sep. 2020.

[24] W. An, S. Xu, and F. Yang, "A metal-only reflectarray antenna using slot-type elements," *IEEE Antennas Wireless Propag. Lett.*, vol. 13, pp. 1553–1556, 2014.

[25] R. Deng, F. Yang, S. Xu, and M. Li, "A low-cost metal-only reflectarray using modified slot-type Phoenix element with 360° phase coverage," *IEEE Trans. Antennas Propag.*, vol. 64, no. 4, pp. 1556–1560, Apr. 2016.

[26] D. Berry, R. Malech, and W. Kennedy, "The reflectarray antenna," *IEEE Trans. Antennas Propag.*, vol. AP-11, no. 6, pp. 645–651, Nov. 1963.

[27] S. V. Polenga, A. V. Stankovsky, R. M. Krylov, A. D. Nemshon, Y. A. Litinskaya, and Y. P. Salomatov, "Millimeter-wave waveguide reflectarray," in *Proc. Int. Siberian Conf. Control Commun. (SIBCON)*, Omsk, Russia, May 2015, pp. 1–4.

[28] Y. G. Antonov, S. V. Ballandovich, G. A. Kostikov, L. M. Liubina, and M. I. Sugak, "Millimeter-wave partially dielectric filled waveguide reflectarray antenna," in *Proc. Antennas Design Meas. Int. Conf. (ADMInC)*, St. Petersburg, Russia, 2019, pp. 107–110.

[29] R. Deng, F. Yang, S. Xu, and M. Li, "A 100-GHz metal-only reflectarray for high-gain antenna applications," *IEEE Antennas Wireless Propag. Lett.*, vol. 15, pp. 178–181, 2016.

[30] H.-T. Chou, C.-Y. Lin, and M.-H. Wu, "A high efficient reflectarray antenna consisted of periodic all-metallic elements for the ku-band DTV applications," *IEEE Antennas Wireless Propag. Lett.*, vol. 14, pp. 1542–1545, 2015.

[31] W. Lee and Y. J. Yoon, "A broadband dual-metallic-reflectarray antenna for millimeter-wave applications," *IEEE Antennas Wireless Propag. Lett.*, vol. 16, pp. 856–859, 2017.

[32] M. Yi, Y. Bae, and S. Yoo, "Millimeter-wave metal reflectarray antennas with sub-wavelength holes," *Electronics*, vol. 10, no. 8, pp. 945–952, Apr. 2021.

[33] Y. H. Cho, W. J. Byun, and M. S. Song, "High gain metal-only reflectarray antenna composed of multiple rectangular grooves," *IEEE Trans. Antennas Propag.*, vol. 59, no. 12, pp. 4559–4568, Dec. 2011.

[34] Y. H. Cho, W. J. Byun, and M. S. Song, "Metallic-rectangular-grooves based 2D reflectarray antenna excited by an open-ended parallel-plate waveguide," *IEEE Trans. Antennas Propag.*, vol. 58, no. 5, pp. 1788–1792, May 2010.

[35] F. Sun, Y. Li, L. Ge, and J. Wang, "Millimeter-wave magneto-electric dipole antenna array with a self-supporting geometry for time-saving metallic 3-D printing," *IEEE Trans. Antennas Propag.*, vol. 68, no. 12, pp. 7822–7832, Dec. 2020.

[36] B. Chen, H. Yi, K. B. Ng, S. Qu, and C. H. Chan, "3D printed reflectarray antenna at 60 GHz," in *Proc. Int. Symp. Antennas Propag. (ISAP)*, Okinawa, Japan, 2016, pp. 92–93.

[37] G. Wu, Y. S. Zeng, K. F. Chan, B. J. Chen, S. W. Qu, and C. H. Chan, "High-gain filtering reflectarray antenna for millimeter-wave applications," *IEEE Trans. Antennas Propag.*, vol. 68, no. 2, pp. 805–812, Feb. 2020.

[38] T. Makdissy, R. Gillard, Z. An, and S. Vaudreuil, "Dual linearly polarised 3D printed phoenix cell for wide band metal only reflectarrays," *IET Microw. Antennas Propag.*, vol. 14, no. 12, pp. 1411–1416, Oct. 2020.

[39] H. Yang et al., "A study of phase quantization effects for reconfigurable reflectarray antennas," *IEEE Antennas Wireless Propag. Lett.*, vol. 16, pp. 302–305, 2017.

[40] P. Mei, S. Zhang, and G. F. Pedersen, "A low-cost, high-efficiency and full-metal reflectarray antenna with mechanically 2-D beam-steerable capabilities for 5G applications," *IEEE Trans. Antennas Propag.*, vol. 68, no. 10, pp. 6997–7006, Oct. 2020.

[41] S. D. Targonski and D. M. Pozar, "Minimization of beam squint in microstrip reflectarrays using an offset feed," in *IEEE AP-S/URSI Int. Symp. Dig.*, Baltimore, MD, USA, 1996, pp. 1288–1291.

[42] E. Almajali, D. A. McNamara, J. Shaker, and R. Chaharmir, "Beam squint suppression in offset-fed reflectarrays," *IEEE Antennas Wireless Propag. Lett.*, vol. 12, pp. 587–590, 2013.

XIAOWEI CAO (Graduate Student Member, IEEE) is currently pursuing the Ph.D. degree with the School of Integrated Circuits and Electronics, Beijing Institute of Technology. His current research interests include leaky-wave antenna design, reconfigurable reflectarray design, and reconfigurable transmitarray design.

CHANGJIANG DENG (Senior Member, IEEE) was born in Loudi, Hunan, China. He received the B.S. degree in communication engineering from Beijing University of Posts and Telecommunications, Beijing, China, in 2011, and the Ph.D. degree in electrical engineering from Tsinghua University, Beijing, in 2016.

He is currently an Associate Professor with the School of Integrated Circuits and Electronics, Beijing Institute of Technology. His research interests include mobile phone antennas, dual polarized antennas, circularly polarized antennas, and MIMO antennas.

YINAN HAO received the B.S. degree in communication engineering from Beijing Institute of Technology, where she is currently pursuing the master's degree with the School of Integrated Circuits and Electronics. Her current research interests include microstrip patch antenna design and reconfigurable reflectarray design.

YOUJIA YIN received the B.S. degree in communication engineering from Beijing Institute of Technology, where he is currently pursuing the Ph.D. degree with the School of Integrated Circuits and Electronics. His current research interests include reconfigurable reflectarray design, and reconfigurable transmitarray design.